THE JOURNAL OF BIOLOGICAL CHEMISTRY
Vol. 272, No. 38, Issue of September 19, pp. 23637–23644, 1997
Printed in U.S.A.


# The A-kinase Anchoring Domain of Type IIα cAMP-dependent Protein Kinase Is Highly Helical*

(Received for publication, June 4, 1997, and in revised form, July 3, 1997)

**Marceen Glavic Newlon‡, Melinda Roy‡, Zachary E. Hausken§, John D. Scott§, and Patricia A. Jennings‡¶**

*From the ‡Department of Chemistry and Biochemistry, University of California, San Diego, La Jolla, California 92093-0359 and the §Howard Hughes Medical Institute, Vollum Institute, Portland, Oregon 97201-3098*

**Subcellular localization of the type II cAMP-dependent protein kinase is controlled by interaction of the regulatory subunit with A-Kinase Anchoring Proteins (AKAPs). This contribution examines the solution structure of a 44-residue region that is sufficient for high affinity binding to AKAPs. The N-terminal dimerization domain of the type IIα regulatory subunit of cAMP-dependent protein kinase was expressed to high levels on minimal media and uniformly isotopically enriched with $^{15}N$ and $^{13}C$ nuclei. Sequence-specific backbone and side chain resonance assignments have been made for greater than 95% of the amino acids in the free dimerization domain using high resolution multidimensional heteronuclear NMR techniques. Contrary to the results from secondary structure prediction algorithms, our analysis indicates that the domain is highly helical with a single 3–5-residue sequence involved in a β-strand. The assignments and secondary structure analysis provide the basis for analyzing the structure and dynamics of the dimerization domain both free and complexed with specific anchoring proteins.**

The protein kinases constitute a diverse family of enzymes with well over one thousand members discovered to date. They differ in substrate specificity (serine/threonine- *versus* tyrosine-specific) as well as in their role in specific signal transduction pathways. Despite this considerable diversity, genetic and structural analyses of the catalytic portions of these enzymes have shown that they evolved from a common ancestor and share a conserved overall fold (1–3). This catalytic core is often flanked by well defined structural domains that confer functional properties upon the enzyme. For example, SH2, SH3, pleckstrin, C1, C2, and Lim domains have been implicated in mediating specific protein-protein or protein-lipid interactions that control specificity and/or alter activity in particular protein kinases (4–6). With this added structural complexity, in many cases it is still unclear how signals from outside the cell reach a specific target in the dense reaches of the cytoplasm and nucleus in a timely fashion. An attractive proposal has recently been raised to address this particular problem. The "targeting hypothesis" proposes that phosphorylation events are controlled, in part, by subcellular localization of protein kinases and phosphatases in the cell via the interaction of targeting domains on the enzymes with specific anchoring proteins (7–10). The principle behind localization is that the protein kinase will be held in close proximity to its target and released when the activation signal is discharged. A pressing issue, then, is to define the molecular basis for these targeting interactions.

The correct intracellular targeting of protein kinases and phosphatases confers specificity to the enzymes, in part, by placing them in close proximity to their preferred substrates. Targeting of these enzymes occurs via association with specific proteins that are found in different locations in the cell (7, 8, 10–12). The classic example of localization of kinase function is the scaffolding of the enzymes involved in the yeast mitogen-activated protein kinase signaling cascade. The pathway is tightly controlled as a result of the interaction of each enzyme in the cascade with a common scaffolding protein, Ste5 (13). Mammalian proteins that serve a similar function are the family of A-Kinase Anchoring Proteins (AKAPs)[1] identified by Scott and co-workers (14, 15). AKAPs maintain the cyclic AMP-dependent protein kinase (PKA) in specific subcellular compartments, thereby ensuring accessibility of the kinase to a limited number of substrates in a particular location (7, 8, 10, 12). This compartmentalization occurs through the interaction of the regulatory domain of PKA with a conserved "anchoring site" on the various AKAPs. The AKAPs also contain a unique "targeting domain" that interacts directly with specific structural proteins, organelles, or membranes.

The current PKA anchoring hypothesis is best described by the model depicted in Fig. 1. The enzyme is an inactive tetramer composed of a regulatory dimer ($R_2$) and two catalytic (2C) subunits ($R_2C_2$) that make up the inactive PKA holoenzyme complex. Binding of the second messenger cAMP to the regulatory subunit dissociates the tetramer to produce the intact $R_2$ dimer and release two catalytically active monomeric C subunits. Localization of PKA occurs through interaction of the AKAP with the N-terminal dimerization domain of the regulatory subunit. The site of RII binding to the AKAPs has been identified for several anchoring proteins, and computer-aided secondary structure prediction has revealed sequences of about 14 residues in Ht31, Ht21, P150, and mitogen-activated protein-2 that have a high probability for amphipathic helix formation (16) that are most likely the RII binding region. A 22-residue peptide mimicking the RII binding site of Ht31 has

* This work was supported by National Institutes of Health Grants GM07313 (to M. G. N.), CA09523 (to M. R.), and DK44239 (to J. D. S. and Z. E. H.) and the Cancer Research Coordinating Committee (to P. A. J.). The costs of publication of this article were defrayed in part by the payment of page charges. This article must therefore be hereby marked "*advertisement*" in accordance with 18 U.S.C. Section 1734 solely to indicate this fact.

¶ To whom correspondence should be addressed.

[1] The abbreviations used are: AKAP, protein kinase A anchoring protein; PKA, cAMP-dependent protein kinase; $R_2$ subunit, cAMP-dependent protein kinase regulatory subunit dimer; C subunit, cAMP-dependent protein kinase catalytic subunit; TOCSY, total correlation spectroscopy; NOE nuclear Overhauser effect; NOESY, nuclear Overhauser enhancement spectroscopy; CSI, chemical shift index; HSQC, heteronuclear single quantum coherence; HMQC, heteronuclear multiple quantum coherence.

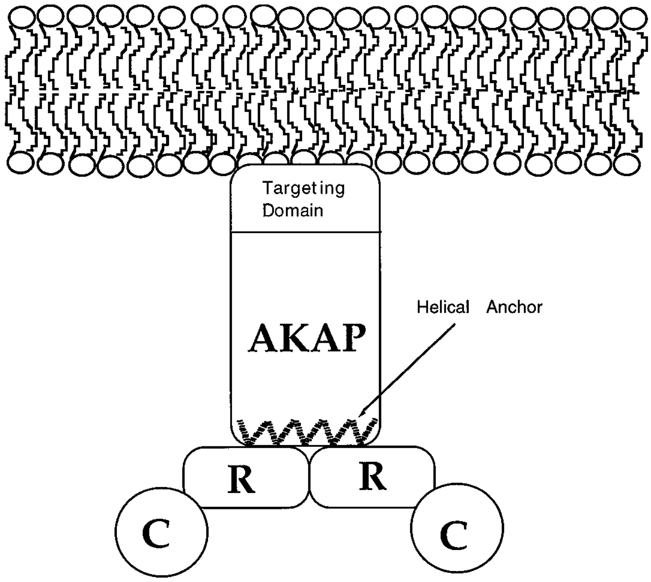


FIG. 1. **Anchoring model.** A schematic model for the anchoring of PKA to a specific subcellular target. The tetrameric holoenzyme associates through its dimeric regulatory subunit with the putative helical anchoring site on the AKAP.

been synthesized which inhibits the binding of full-length Ht31 binding to RII (17).

Although x-ray crystallographic analysis has been successful in elucidating the structure of a fragment that encompasses the cAMP binding domains of the regulatory subunit (18), until this time there was no structural information on the dimerization and AKAP binding regions. We bacterially expressed, isotopically enriched, and purified the 44-residue dimerization domain of the type $II_\alpha$ $R_2$ subunit ($RII_\alpha$-(1–44)). This region is highly stable and binds anchoring proteins and peptides with nanomolar affinity (19, 20). In this article, we report the $^1$H, $^{15}$N, and $^{13}$C backbone resonance assignments and secondary structure analysis of uniformly $^{15}$N and $^{13}$C isotopically enriched $RII_\alpha$-(1–44) as determined by multidimensional heteronuclear NMR techniques.

## EXPERIMENTAL PROCEDURES

*Purification of $RII_\alpha$-(1–44)*—The plasmid encoding the gene for recombinant $RII_\alpha$-(1–44) was inserted into the pET16b (Novagen, Inc.) expression vector. This construct allows for the rapid purification of the expressed protein by $Ni^{2+}$ affinity chromatography. The intact RIIα domain is released from the N-terminal His-tag by factor Xa cleavage (21, 22). The expression plasmid was transformed into *Escherichia coli* BL21 (DE3) cells. 1 liter of media (either Luria-Bertani broth (LB) for obtaining unlabeled $RII_\alpha$-(1–44) or minimal media supplemented with 2.5 g/liter [$^{13}$C]glucose and/or 2.0 g/liter [$^{15}$N]ammonium sulfate (Isotech, Inc.) for obtaining $^{15}$N/$^{13}$C-enriched $RII_\alpha$-(1–44)) containing 150 mg/ml ampicillin is inoculated with a 5-ml starting culture of *E. coli*. The 1-liter culture is grown at 37 °C to an $A_{600}$ of 0.5 prior to induction with 1 mM isopropyl β-D-thiogalactoside. Cells are harvested by centrifugation for 45 min at 7,000 × *g*.

The cells are resuspended in 40 ml of buffer A (5 mM imidazole, 0.5 M NaCl, 20 mM Tris-HCl, pH 7.9, 4 °C) and lysed by sonication. The cellular debris is collected by centrifugation at 30,000 × *g*. $RII_\alpha$-(1–44) grown in LB media is expressed as inclusion bodies, which are solubilized and unfolded using 5 ml of 6 M guanidine HCl for 1 h at 25 °C. The protein is refolded by slow dilution with 25 ml of buffer A containing 1 M imidazole over 2 h, followed by subsequent dialysis into buffer A at 4 °C. $RII_\alpha$-(1–44) grown in minimal media is found in the soluble fraction.

The dialysate or supernatant was applied to a nickel chelating column (Novagen, Inc.) equilibrated in buffer A. The column is washed with 3 column volumes of buffer A and 10 column volumes of buffer A containing 60 mM imidazole to remove any nonspecifically bound protein. The RIIα His-tag fusion protein is eluted in 20 ml of buffer A with 1 M imidazole and concentrated to 10 ml by Centriplus (Amicon, Inc.). The protein is then exchanged into buffer B (20 mM Tris-HCl, 100 mM NaCl, 2 mM $CaCl_2$, pH 8.0) using a PD-10 column (Pharmacia Biotech Inc.).

Release of $RII_\alpha$ from the fusion protein is accomplished by incubating 25 mg of factor Xa (New England Biolabs, Inc.) for every 8 mg of $RII_\alpha$-(1–44). The reaction mixture is incubated overnight at 37 °C with shaking. The efficiency of the cleavage reaction is ~90%, as judged by sodium dodecyl sulfate-polyacrylamide gel electrophoresis. A Superdex 75 HiLoad 16/60 (Pharmacia) 120-ml gel filtration column equilibrated in 20 mM sodium phosphate buffer, pH 4.0, separated the factor Xa and the cleaved His-Tag from the RIIα protein. Purified $RII_\alpha$-(1–44) eluted at 70 ml and was concentrated by Centriplus (Amicon, Inc.). The purified $RII_\alpha$-(1–44) contains two additional N-terminal amino acids (designated $His^{-1}$-$Met^0$) as a result of the vector construction (Novagen, Inc.).

The protein concentration was determined at a wavelength of 278 nm using an extinction coefficient of 2800 $M^{-1}$ $cm^{-1}$ obtained from the method of Gill and von Hippel (23). $RII_\alpha$-(1–44) was >95% pure as determined from SDS-polyacrylamide gel electrophoresis analysis. Complete cleavage of the fusion protein was confirmed by electrospray ionization mass spectrometric analysis.

*NMR Experiments*—All NMR experiments were performed at 25 °C on either a Bruker DMX500 or a DRX600 spectrometer using a triple resonance gradient probe. Optimal NMR conditions were determined from a two-dimensional homonuclear TOCSY (24) pH titration performed on a 2 mM (dimer concentration) unlabeled sample of $RII_\alpha$-(1–44) in 20 mM sodium phosphate buffer, 90% $H_2O$, 10% $D_2O$. The $^1$H spectral widths were 5000 Hz (10 ppm) in both $t_2$ and $t_1$. 2K by 512 point matrices were collected. Water suppression was achieved through a WATERGATE sequence (25, 26). An MLEV-17 (24) sequence of 59.3 ms was used for the TOCSY spin lock. The optimal pH was determined as pH 4 to be used in further NMR experiments.

Typically, the isotopically enriched NMR samples were prepared at a dimer concentration of 1 mM (2 mM monomer) in 20 mM sodium phosphate buffer, 90% $H_2O$, 10% $D_2O$, pH 4.0. The $^1$H chemical shift of water was 4.755 ppm when referenced to sodium 2,2-dimethyl-2-silapentane-5-sulfonate, whereas $^{15}$N and $^{13}$C were indirectly referenced to sodium 2,2-dimethyl-2-silapentane-5-sulfonate, as established by Wishart *et al.* (27). Quadrature phase detection in the indirectly detected dimensions for all experiments was obtained via time proportional phase incrementation (28), except for the CBCA(CO)NH and HNCACB experiments, which utilized States (29) for the $^{13}$C dimension and sensitivity-enhanced gradient-detected echo/antiecho (30–32) in the $^{15}$N dimension.

Using the same unlabeled protein sample as described for the two-dimensional TOCSY experiments, a two-dimensional homonuclear NOESY (33) experiment was collected with a mixing time of 200 ms. The $^1$H spectral widths were 5000 Hz (10 ppm) in both $t_2$ and $t_1$. A 4K by 512 point matrix was collected. Water suppression was achieved through the WATERGATE sequence (25, 26).

The two-dimensional $^1$H-$^{15}$N heteronuclear single quantum coherence (HSQC) experiment (34, 35), the three-dimensional $^1$H-$^{15}$N NOESY-HSQC (36), and the three-dimensional $^1$H-$^{15}$N TOCSY-HMQC (36) were acquired on a uniformly enriched $^{15}$N protein sample, pH 4.0. In the HSQC and the NOESY-HSQC experiments, the $^1$H carrier during the evolution of the $^{15}$N and $^1$H dimensions was centered at the water frequency but was shifted to 8.045 ppm before acquisition. In the TOCSY-HMQC experiment, the $^1$H carrier was placed on the water frequency throughout the entire experiment. In all three experiments the $^{15}$N carrier was placed at 117.5 ppm. Mixing times of 150 and 200 ms were used for the NOESY-HSQC, while the TOCSY-HMQC experiments were run at spin-lock times of 40.5, 81.0, and 101.3 ms. Water suppression for the HSQC and NOESY-HSQC was accomplished using the gradient tailored WATERGATE sequence (25, 26). A presaturation pulse was employed to suppress the water in the TOCSY-HMQC. Broadband $^{15}$N decoupling for the three $^1$H-$^{15}$N experiments was accomplished using a WALTZ16 decoupling scheme (37). In the two-dimensional HSQC experiment, 128 real $t_1$ ($^{15}$N) and 512 complex $t_2$ ($^1$H) points were collected with spectral widths corresponding to 1773 Hz (35 ppm) ($t_1$) and 3005 Hz (6 ppm) ($t_2$). For the three-dimensional $^1$H-$^{15}$N experiments, a total of 128 real $t_1$ ($^1$H), 64 real $t_2$ ($^{15}$N), and 512 complex $t_3$ ($^1$H) points were collected. The spectral widths were 4999 Hz (10 ppm) ($t_1$), 1773 Hz (35 ppm) ($t_2$), and either 5000 (10 ppm) or 3005 Hz (6 ppm) ($t_3$).

The three-dimensional CBCA(CO)NH (30, 38), the three-dimensional HNCACB (30, 39), the three-dimensional CT-HNCA (40), the three-dimensional CT-HN(CO)CA (41), and the three-dimensional HCCH-TOCSY (42, 43) were acquired on a uniformly $^{15}$N-$^{13}$C enriched protein sample at pH 4.0. The $^1$H carrier was either placed at the water

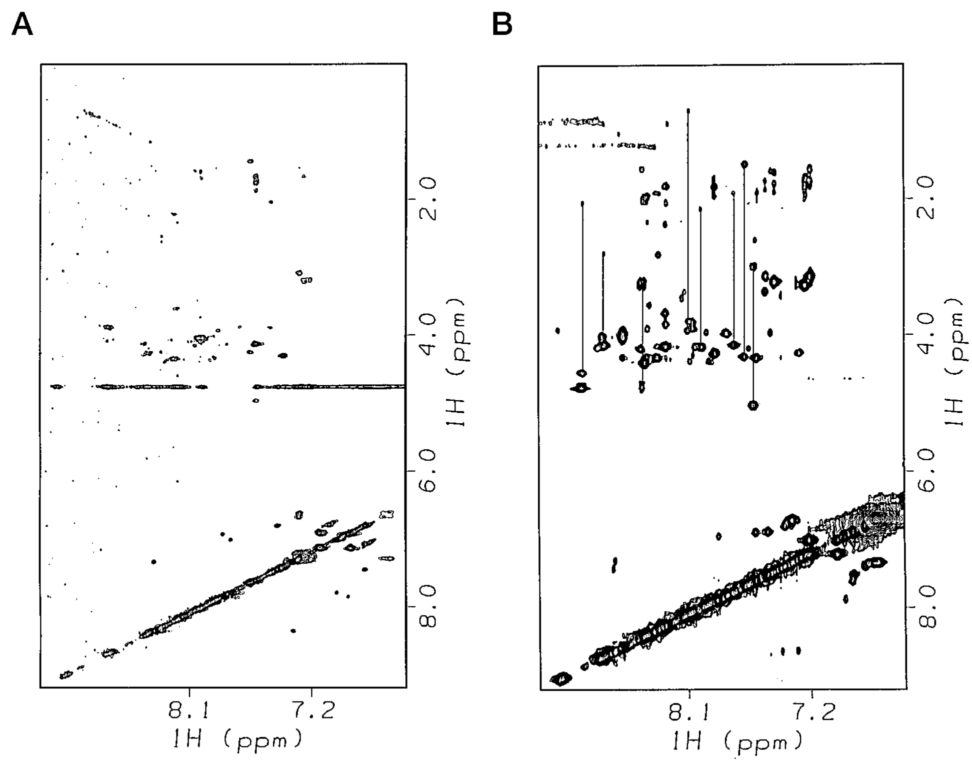


FIG. 2. **Comparison of the two-dimensional TOCSY spectra of RII$\alpha$-(1–44) recorded at pH 7.0 (*A*) and pH 4.0 (*B*).** Except for pH, the sample conditions were identical with a mixing time of 60 ms. In the pH 4.0 spectrum, several of the correlations that are missing in the pH 7.0 spectrum are indicated.

frequency throughout the entire experiment (HNCACB, CBCA-(CO)NH), shifted to 8.045 ppm (HNCA, HN(CO)CA), or shifted to 2.407 ppm (HCCH-TOCSY) prior to data acquisition. The $^{15}$N carrier was placed at 117 ppm for all triple resonance experiments, and the $^{13}$C carrier was set to either 42.3 (HNCACB and HCCH-TOCSY) or 57.3 ppm (HNCA and HN(CO)CA). For the CBCA(CO)NH experiment, the $^{13}$C carrier originated at 42.3 ppm but once the magnetization was transferred to $^{13}$C′, the carrier was shifted to 177.3 ppm. The WATERGATE sequence (25, 26) was used to suppress the water signal in the CT-HNCA, CT-HN(CO)CA, and HCCH-TOCSY experiments. When the $^{13}$C carrier was at 42.3 ppm, $^{13}$C′ pulses were achieved using off-resonance phase-shifted laminar pulses (44). WALTZ16 (37) and SEDUCE-1 (45, 46) pulse sequences were used for broadband $^{1}$H, $^{15}$N, and $^{13}$C decoupling. The total number of points collected for the CBCA(CO)NH and HNCACB experiments was 38 or 52 complex $t_1$ ($^{15}$N), 52 complex $t_2$ ($^{13}$C), and 1024 complex $t_3$ ($^{1}$H), and the spectral widths were 1520 Hz (25 ppm)($t_1$), 10564 Hz (70 ppm)($t_2$), and 7184 Hz (12 ppm) ($t_3$). In the HNCA and HN(CO)CA experiments, 64 real $t_1$ ($^{13}$C), 48 or 50 real $t_2$ ($^{15}$N), and 512 complex $t_3$ ($^{1}$H) points were collected at spectral widths of 3771 Hz ($t_1$), 1266 (25 ppm) or 1367 Hz (27 ppm) ($t_2$), and 3005 Hz (6 ppm) ($t_3$). The HCCH-TOCSY experiment was acquired with 128 real $t_1$ ($^{1}$H), 110 real $t_2$ ($^{13}$C), and 512 complex $t_3$ ($^{1}$H) points and 4999 Hz (10 ppm) ($t_1$), 8400 Hz (67 ppm) ($t_2$), and 3005 Hz (6 ppm) ($t_3$) spectral widths.

Amide proton exchange experiments were carried out on a 0.5 mM protein sample originally in 20 mM sodium phosphate buffer, 90% $H_2O$, 10% $D_2O$, pH 4.0, which was exchanged into 20 mM deuterated sodium phosphate buffer, 100% $D_2O$ pD 3.5, using Quick Spin™ Protein Columns (Boehringer Mannheim). Two-dimensional HSQC experiments, matrix size 512 × 64, were run at times of 10 and 30 min, 2, 7, and 25 h after exchange into $D_2O$.

All experiments were processed using Felix 95.0 software (MSI, San Diego, CA) using an Indigo-2 workstation (Silicon Graphics, Inc.). The data were apodized with a squared sinebell function shifted by 70° in all dimensions before Fourier transformation. For all three-dimensional experiments linear prediction to an additional one-third of the number of points collected was applied before apodization in both $t_1$ and $t_2$.

*Circular Dichroism Spectroscopy*—Circular dichroism (CD) spectra were measured at pH values 4.0 and 7.0 in 20 mM sodium phosphate buffer at 25 °C. CD spectra were obtained on an Aviv 61DS spectropolarimeter (Aviv Associates) calibrated with a standard solution of 10-camphorsulfonic acid (47, 48). Spectra were measured with a 0.5-nm bandwidth, 0.5-nm step size, and a 1.0-s time constant over a wavelength range of 260 to 180 nm in 0.1-cm optical cells.

*Gel Filtration Chromatography*—Gel filtration chromatography was performed on a TSKGel G2000SW column (Tosohaas, Inc.), 30 cm by 7.8 mm. 50 $\mu$l of a 0.8 mg/ml RII$_{\alpha}$-(1–44) sample was injected onto the column equilibrated in 20 mM phosphate, 100 mM NaCl, pH 4.0, at a flow rate of 0.5 ml/min. The column was calibrated with standard proteins corresponding to molecular masses of 670, 158, 44, 17, and 1.35 kDa (Bio-Rad, Inc.).

## RESULTS

*Optimizing NMR Conditions*—At pH 7.2, the two-dimensional $^{1}$H-$^{15}$N HSQC experiment of RII$_{\alpha}$-(1–44) displays a well dispersed spectrum (data not shown). Fig. 2*A* shows that at this same pH, the efficiency of the TOCSY transfer in the two-dimensional homonuclear TOCSY is extremely poor. The data in the TOCSY experiment were greatly improved as the pH was varied from pH 7 to pH 4, as seen in Fig. 2*B*. It is evident from these NMR spectra that as the pH of the sample decreases, the protein becomes more amenable to study by NMR methods.

One concern with doing NMR studies at pH 4 is that significant structural changes may accompany the change in solution conditions. To address this issue, we examined two parameters. First we found that the aliphatic proton resonances do not shift upon variation of pH (data not shown). Second, circular dichroism (CD) analysis was performed. A comparison plot of the mean residue ellipticity of the protein at pH values 4.0 and 7.0 as a function of wavelength is given in Fig. 3. The spectra show the classic double minima at 210 and 222 nm expected for helical structure in solution (49). In addition, the spectra of the domain were identical at pH 4.0 and 7.0 (Fig. 3), indicating no gross structural changes occur as a result of the change in solution conditions. Our CD results indicate the presence of significant helical structure (~50%) (49), consistent with our interpretation of the NMR data (see "Discussion").

Dynamic light scattering results indicate a decrease in the apparent molecular weight upon decreasing pH, suggesting a

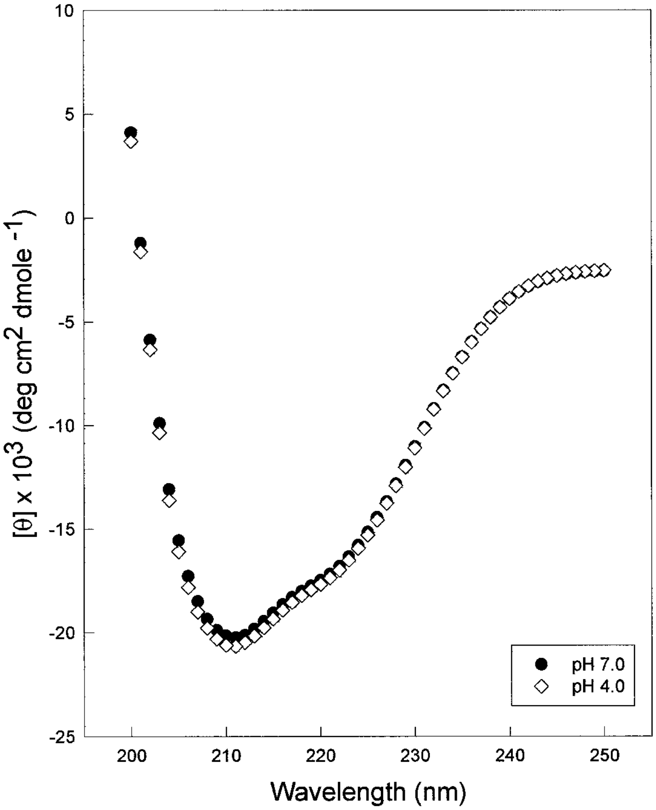


FIG. 3. **Comparison of the CD spectra of RIIα-(1–44) at pH values 7.0 and 4.0.** CD spectra of RIIα-(1–44) were measured as described under "Experimental Procedures."

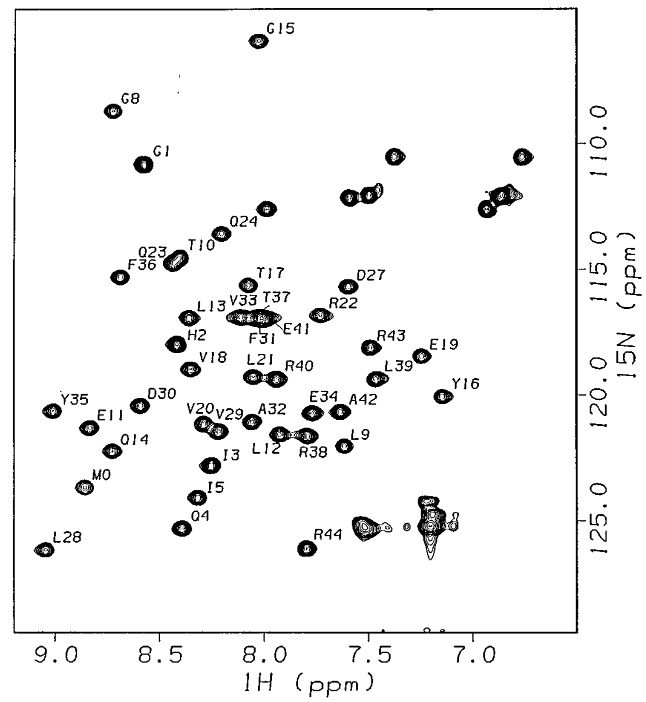


FIG. 4. **Complete $^{1}$H, $^{15}$N HSQC spectrum of RIIα-(1–44) at 25 °C, pH 4.0.** All backbone amide resonances are identified. Cross-peaks due to the side chains of glutamine are not labeled (there are no asparagine residues in this sequence).

reduction in non-native protein association into higher order oligomers. The minimum apparent molecular weight observed by this technique is in the pH range of 3 to 4. Gel filtration chromatography demonstrates the presence of a single species at pH 4.0 with the apparent molecular weight expected for dimeric $RII_{\alpha}$-(1–44) (data not shown). TOCSY observations also indicate a reduction in the amount of nonspecific protein association upon decreasing pH. Aliphatic proton linewidths at pH 4.0 are consistent with a dimeric system (results not shown).

Based on the increase in magnetization transfer, the observation of a single species by gel filtration chromatography, a molecular weight consistent dimeric $RII_{\alpha}$-(1–44), and line widths typical of an 11-kDa protein, a pH of 4.0 was chosen as optimal for further NMR spectroscopic structural studies. At this pH, the integrity of the AKAP interaction is still intact according to RII overlay techniques (50) and analysis of peptide binding by NMR at pH 7.0 and 4.0.[2] A significant amount of biochemical data demonstrates dimerization of RII is essential for AKAP binding (19, 51, 52), confirming the presence of dimer in our present study.

*Resonance Assignments*—The two-dimensional $^{1}$H-$^{15}$N HSQC of $RII_{\alpha}$-(1–44) is shown in Fig. 4. All 41 non-proline backbone resonances that were expected (excluding the N-terminal histidine) were observed. The number of cross-peaks in this experiment is equivalent to the number of backbone resonances expected for the monomer of $RII_{\alpha}$-(1–44), which suggests a stable, symmetric homodimer conformation. The difficulty in distinguishing inter- from intraresidue NOE cross-peaks in a dimeric system led us to use triple resonance techniques to complete sequential backbone resonance assignments. Comparison of the intraresidue $^{1}H^{N}$, $^{15}$N to $^{13}C\alpha/^{13}C\beta$ connectivities observed in the CT-HNCA and the HNCACB three-dimensional spectra with the sequential intraresidue $^{1}H^{N}$, $^{15}$N to $^{13}C\alpha/^{13}C\beta$ connectivities observed in CBCA(CO)NH and CT-HN(CO)CA data allowed nearly complete identification of sequential connectivities. A series of the $^{1}H^{N}$, $^{15}$N to $^{13}C\alpha$ connectivities obtained in the CT-HNCA experiment for residues 8–17 is presented in Fig. 5. The combined spectra allowed for assignment of $^{15}$N and $^{1}H^{N}$ resonances for 41 of 42 expected residues (98% of backbone amides), $^{13}C^{\alpha}$ and $^{1}H^{\alpha}$ resonances for 44 of 46 (96%) residues, and $^{13}C^{\beta}$ and $^{1}H^{\beta}$ for 41 (93%) of the non-glycine residues. $^{13}C^{\alpha}$ chemical shifts used in secondary structure prediction (see below) were measured with the higher resolution CT-HNCA and CT-HN(CO)CA experiments.

Side chain spin systems were identified either completely or partially from the TOCSY-HMQC and HCCH-TOCSY data. The TOCSY-HMQC experiment provided information of only $^{1}H^{\alpha}$ and $^{1}H^{\beta}$ resonances, whereas the improved magnetization transfer afforded by the HCCH-TOCSY experiment was able to identify the majority of the side chain $^{1}$H and $^{13}$C resonances that remained, approximately (85%), and confirmed existing assignments. The HCCH-TOCSY established the assignment of $^{13}C^{\alpha}$ and $^{1}H^{\alpha}$ resonances of $Pro^{6}$ and $Pro^{25}$, which were not probed in any other heteronuclear experiment, and $^{1}H^{\delta}$ resonances of all four of the proline residues were identified by combining information obtained by the HCCH-TOCSY experiment and the two-dimensional homonuclear NOESY experiment.

## DISCUSSION

*Secondary Structure Determination*—Elucidating the structure of the N-terminal anchoring domain of RIIα is an essential first step toward understanding the mechanisms of localization and anchoring of PKA. The lack of structural information and sequence homology to other proteins whose structures are known prompted us to initiate NMR studies of this domain. We expressed $RII_{\alpha}$-(1–44) to high levels on minimal media and

[2] M. Newlon and P. A. Jennings, manuscript in preparation.

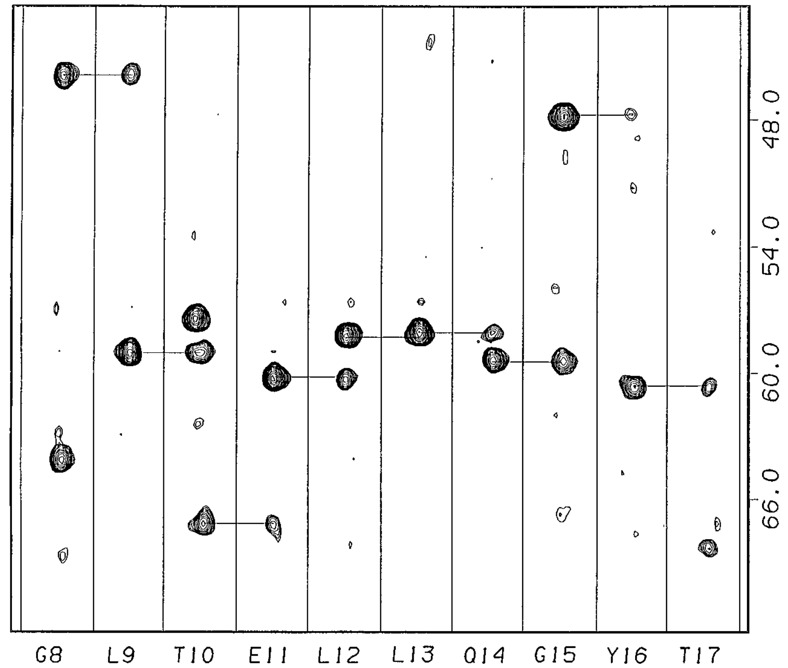


FIG. 5. **Correlation of residues Gly[8]-Thr[17] of RII$\alpha$-(1–44) from the three-dimensional CT-HNCA experiment.** The strips were originally selected from a two-dimensional $^{1}$H-$^{15}$N HSQC which selected the $^{1}$H and $^{15}$N resonances. Sequential residues are identified by *horizontal lines*. The extra peaks for strip Thr[10] are due to overlapping $^{1}$H and $^{15}$N chemical shifts of Thr[10] and Gln[23] (see Fig. 4). The strip of Leu[13] contains only one peak because of degenerate $^{13}C^{\alpha}$ chemical shift of Leu[12] and Leu[13].

uniformly isotopically enriched it with $^{15}$N and $^{13}$C nuclei. This region is sufficient for high affinity binding to AKAPs (19, 20). We now report the first structural information for this domain.

Initial evaluation of secondary structure conformation in RII$\alpha$ was accomplished by determining the $^{13}C^{\alpha}$ chemical shifts and comparing them to random coil chemical shift information (53–56). The chemical shift index (CSI) method is based on the consideration that the $\Phi$, $\Psi$ angles change with $\beta$-sheet and $\alpha$-helix conformations, which result in characteristic changes in $^{13}$C chemical shifts. Although $^{13}C^{\alpha}$, $^{13}C^{\beta}$, and $^{1}H^{\alpha}$ chemical shifts are all useful probes, the most accurate measure of secondary structure elements by this method is the $^{13}C^{\alpha}$ chemical shift. Wishart *et al.* (55) have determined that $^{13}C^{\alpha}$ resonances that shift downfield relative to random coil values are a result of $\alpha$-helical structure formation, whereas upfield shifts indicate the presence of $\beta$-strand. The $C^{\alpha}$ secondary shifts of RII$\alpha$-(1–44) (observed chemical shifts minus random coil chemical shifts) are assigned a value of +1 for shifts > +0.7 ppm, a value of −1 for shifts < −0.7 ppm, and a value of 0 for shifts > −0.7 but < +0.7 ppm relative to the random coil chemical shifts. The data obtained for RII$\alpha$-(1–44) are plotted as a function of residue number in Fig. 6. This secondary shift data indicates that RII$\alpha$-(1–44) contains two $\alpha$-helices and one $\beta$-strand in each monomer of the dimeric protein.

Data obtained in NOE spectra are a direct observation of residue interactions. Regions typical of either $\beta$-strand, $\alpha$-helix, or $\beta$-turn show characteristic NOE cross-peaks (57). The three-dimensional NOESY-HSQC was analyzed conservatively based on the initial through-bond sequential assignments. The NOE cross-peaks observed in $RII_{\alpha}$-(1–44) confirm the $^{13}C^{\alpha}$ secondary shift data presented in Fig. 6. Intense $d_{NN}$, $d_{\beta N(i,\, i+1)}$ and weak $d_{\alpha N(i,\, i+3)}$ cross-peaks, which are all characteristic of $\alpha$-helical structures, were detected for a large portion of the molecule, including Leu[9] through Gln[23] and Leu[28] through Ala[42]. This consistency is especially important for a dimeric protein because the NOE data by itself, which is a direct observation of secondary structure, can be overinterpreted due to the presence of intramolecular as well as intermolecular NOE signals (58–61).

*$\alpha$-Helical Structures*—In contrast to secondary structure prediction algorithms, $RII_{\alpha}$-(1–44) demonstrates a high proportion of $\alpha$-helix when analyzed by circular dichroism (Fig. 3) as well as NMR spectroscopy. The two $\alpha$-helical regions span residues Leu[9]-Gln[23] (helix I) and Leu[28]-Ala[42] (helix II) as observed from strong $d_{NN}$ and $d_{\beta N(i,\, i+1)}$ cross-peaks and medium intensity $d_{\alpha N(i,\, i+3)}$ cross-peaks as well as $^{13}C^{\alpha}$ secondary shift analysis (Fig. 6). Residue Gln[24] is not included in the C-terminal end of the first helix because of the lack of $d_{\alpha N(i,\, i+3)}$ NOE cross-peaks and the change in CSI characterization to $\beta$-strand at this residue (indicative of a change in secondary structure) (54), although a $d_{NN}$ cross-peak with Gln[23] still exists.

Hydrogen exchange experiments were used to detect slowly exchanging amide protons in RII$\alpha$. Twenty-five amide protons show protection from amide proton exchange with solvent, and 12 out of 41 possible amide protons were still observed after 25 h in $D_2O$ (data not shown). Amide protons that exchange slowly are either buried inside the protein or involved in hydrogen bonding interactions, thereby implying stable secondary structure elements. The slowly exchanging protons in $RII_{\alpha}$-(1–44) lie in the regions defined as $\alpha$-helical from both the NOESY and CSI method (Fig. 6).

Consideration of $^{13}C^{\alpha}$ chemical shift and NOE data indicates 65% of the protein is involved in helical interactions, and CD experiments indicate 50% helical content. Although the CD results provide a qualitative assessment of secondary structure content, the contributions of aromatic amino acids in the far UV-CD (62) as well as the reduction in signal as a result of non-optimal alignment of the carbonyl groups if the helices are frayed (49, 62) will result in an underestimation of the helical content of a protein in solution by CD methods.

Indeed, helical fraying is apparent from the exchange rates when compared with the intrinsic exchange rate for the particular amino acid at pD 3.5 and 25 °C. The rate of hydrogen-deuterium isotope exchange of the amide protons of residues located at the center of the helices are much slower than those observed for protons lying on both ends of the helices (Fig. 6). These data indicate that the ends of the helices are less likely to be involved in stable hydrogen bonding interactions (63, 64). Estimation of stable helical content from hydrogen exchange predicts 54% of the protein is involved in stable hydrogen bonding interactions (helical structure), in line with our CD results. Thus it appears that helical fraying is affecting the CD

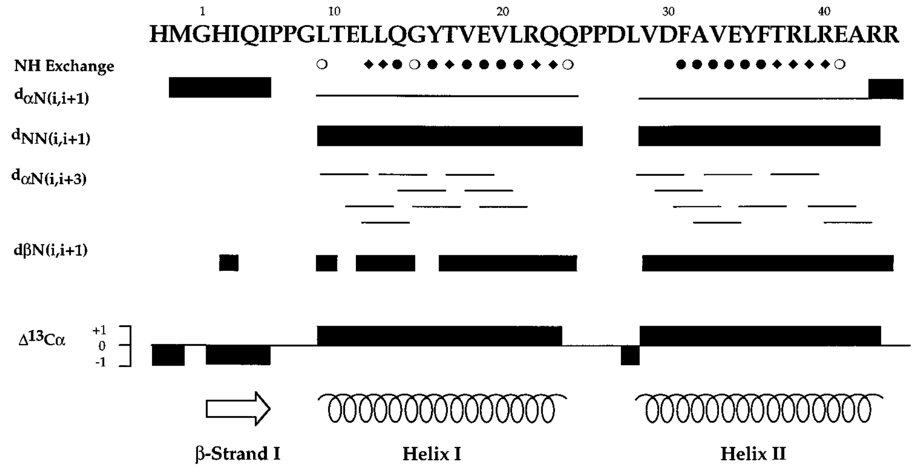


FIG. 6. **Representation of the NOE contacts, $^{13}C^{\alpha}$ chemical shifts, and NH exchange data that are relevant for secondary structure prediction.** *Open circles, filled diamonds*, and *filled circles* represent those amide protons still present after 2, 7, and 25 h in $D_2O$, respectively (all significant when compared with intrinsic exchange rates). The chemical shift differences, based on the CSI method that assigns a +1 to the residue if it falls downfield of the random coil value ±0.7 ppm (helical), or −1 to the residue if it falls upfield of the random coil value ±0.7 ppm (β-sheet), are reported for $^{13}C^{\alpha}$. Regions corresponding to β-strand and α-helix are indicated.

spectrum. A more detailed hydrogen exchange study is currently in progress.

*β-Turns*—There are two regions of the sequence that show β-turn-like behavior in $RII_{\alpha}$-(1–44). The region that encodes $Pro^6$-$Pro^7$-$Gly^8$-$Leu^9$ is a proposed β-turn based on the change in $^{13}C^{\alpha}$ chemical shift from β-strand to random coil ($Ile^5$ to $Gly^8$) and the presence of NOE cross-peaks characteristic of β-turns. The HCCH-TOCSY data allowed the identification of the $^{13}C^{\alpha}$ and $^1H^{\alpha}$ resonances of $Pro^7$, which were important for defining the conformation of this turn. The distances between the $^1H^{\alpha}$ of residue i and the $^1H^N$ of residue i + 1 ($d_{\alpha N(i,\ i+1)}$) and $^1H^{\alpha}$ of residue i and the $^1H^N$ of residue i + 2 ($d_{\alpha N(i,\ i+2)}$) in a type II β-turn are 2.2 and 3.3 Å, respectively (57). The turn appears to adopt a type II β-turn configuration due to the observation of an intense $d_{\alpha N(i,\ i+1)}$ cross-peak for residues $Pro^7$ and $Gly^8$, a weaker $d_{\alpha N(i,\ i+2)}$ cross-peak for $Pro^7$ and $Leu^9$, and a medium intensity $d_{NN(i,\ i+1)}$ cross-peak between $Gly^8$ and $Leu^9$. The hydrogen-deuterium exchange rate of the backbone amide of $Leu^9$ is much slower than the intrinsic exchange rate at this pH (65–67) and that observed for the surrounding residues, so the existence of a hydrogen bond between the amide proton of $Leu^9$ with the carbonyl oxygen of $Pro^6$ is proposed. Studies on linear peptides containing the sequence N-Ac-Pro-Gly-*X*-OH, where *X* is Gly, Ala, Leu, or Ile, occur in type II turns (68), consistent with our proposal.

The sequence defined by residues $Pro^{25}$-$Leu^{28}$ constitutes the second turn. The second turn demonstrates a change in the $^{13}C^{\alpha}$ chemical shift from α-helix at $Gln^{23}$ to β-strand at $Gln^{24}$ and $Asp^{27}$. Again, two prolines lie in this region, and partial side chain identification of the prolines has been determined. We propose the second turn is formed by the residues $Pro^{25}$-$Pro^{26}$-$Asp^{27}$-$Leu^{28}$. The NOE cross-peaks and $H^N$ exchange data suggest a type I turn conformation. Significant NOE cross-peaks involved in determining this turn include a weak $d_{\alpha N(i,\ i+1)}$ cross-peak observed between $Pro^{26}$ and $Asp^{27}$, a medium $d_{\delta N(i,\ i+1)}$ cross-peak between $Pro^{26}$ and $Asp^{27}$, a medium $d_{NN(i,\ i+1)}$ between $Asp^{27}$ and $Leu^{28}$, and a strong $d_{\alpha N(i,\ i+1)}$ cross-peak between $Asp^{27}$ and $Leu^{28}$. A weak $d_{\alpha N(i,\ i+2)}$ NOE cross-peak between $Asp^{27}$ and $Val^{29}$ suggests that helix II starts with $3_{10}$ helix behavior and then turns into regular α-helical structure.

It is worth restating at this time that intermolecular NOE cross-peaks can be observed in this dimer, which may be confusing the identification of this turn. There are also no residues in this region of the sequence that show slow amide exchange rates indicative of the presence of stable hydrogen bonds. Interestingly, the only difference in the sequence between the first and second turn is the replacement of a glycine for an aspartic acid residue (Fig. 6); thus, consistent with the detailed work of Dyson and co-workers (69–72), this replacement is likely affecting the conformation of the turn.

Data obtained from two-dimensional heteronuclear NOESY experiments reveal that at least three of the four of the proline residues are involved in trans-peptide bonds with its preceding residue. No strong $d_{\alpha\alpha(i,\ i+1)}$ for the sequence $Xaa^i$-$Pro^{i+1}$ were observed, which would indicate a cis-peptide bond, but in the cases of $Pro^7$, $Pro^{25}$, and $Pro^{26}$, strong $d_{\alpha\delta(i,\ i+1)}$ cross-peaks are observed, which are indicative of trans-peptide bonds (57) .

*β-Strand*—The presence of β-strand structure in $RII_{\alpha}$-(1–44) is low. The residues $Gly^1$-$Ile^5$ show the only β-strand characteristic intense $d_{\alpha N(i,\ i+1)}$ cross-peaks and the residues $Ile^3$-$Ile^5$ correspond to a β-strand motif using the CSI method as well. The residues $Ile^3$ and $Ile^5$, which have been implicated in AKAP binding by mutagenesis (19), reside in this β-strand region.

*Structural Implications*—Mutagenesis experiments indicate that the side chain of $Phe^{36}$ in helix II is critically important for dimer formation (52). The side chain of this residue shows medium range NOE cross-peaks to $Val^{20}$ in helix I. $Val^{20}$ also shows intense side chain NOE cross-peaks to $Phe^{31}$ (data not shown). Helical wheel projections (Fig. 7*A*) indicate that $Phe^{31}$ and $Phe^{36}$ are 1½ turns away from one another and lie on opposite sides of helix II, suggesting that one of these contacts with $Val^{20}$ must be intermolecular. If our current model of two helices separated by a tight hairpin turn is correct, this would place $Val^{20}$ near $Phe^{31}$ as an intrasubunit contact, and the contact of $Val^{20}$ with $Phe^{36}$ would then be across the two subunits.

Mutagenesis experiments also implicate other residues important for dimerization. The side chain of $Leu^{13}$ is critical for dimer formation (52). This residue resides on the same side of helix I as $Val^{20}$, which would place it on the same face of the helix that interacts with $Phe^{36}$ in the intersubunit contact. Additional studies have shown that the first 10 residues are also important for dimer formation (19, 73). We propose that $Leu^9$, which is located on the same interface of helix I as $Val^{20}$ (Fig. 7*A*), may be responsible for this important dimer contact.

A cartoon of a possible protomer conformation is given in Fig. 7*B*. Although not necessarily a representation of the tertiary fold, this model gives some insight into the available mutagenesis data that demonstrate residues $Ile^3$ and $Ile^5$ located on the N-terminal β-strand, (19, 73) are necessary for AKAP targeting. Mutagenesis of $Pro^7$ to Ala, which changes the AKAP binding specificity of RIIα to that of RIIβ (73), lies in the turn between this β-strand and helix I. This mutation may alter the packing of the strand in respect to the helix or cause slight alterations in the relative orientations of these helices. Similarly, $Pro^{26}$ in the turn region of RIIα is also an Ala in RIIβ which also may be a target for AKAP binding specificity by

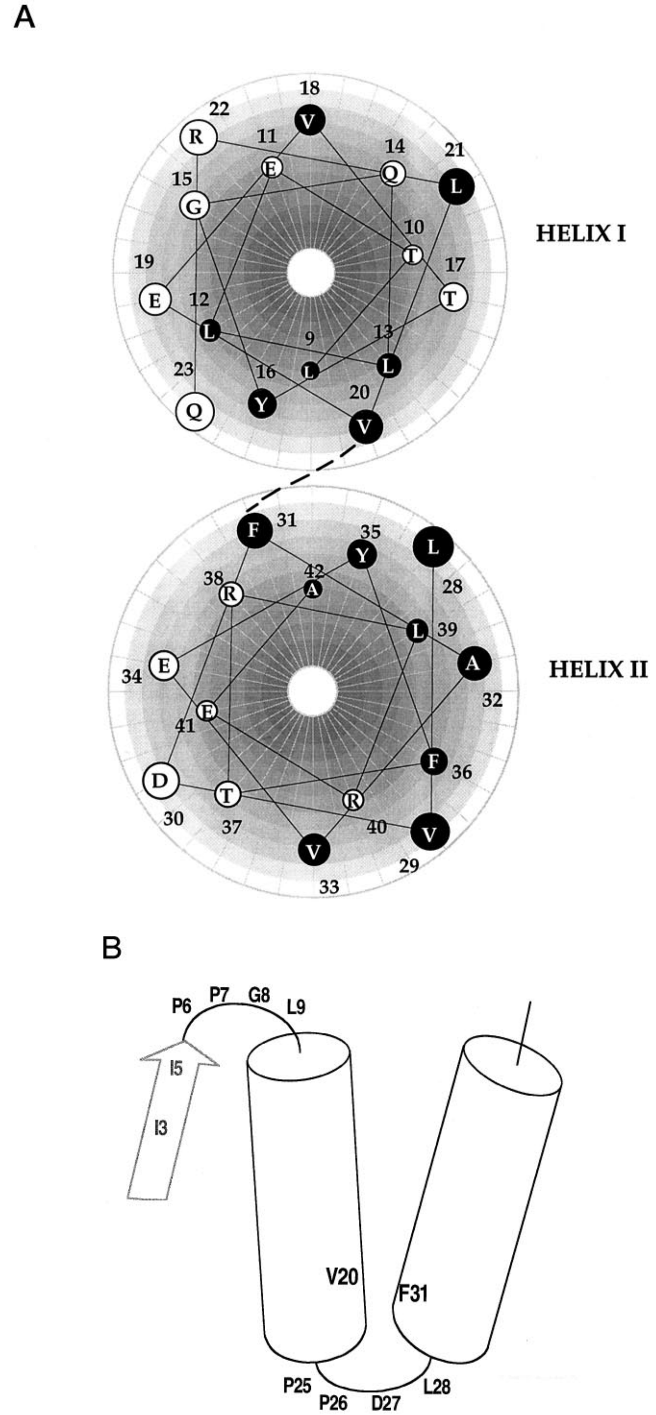


FIG. 7. **Helical wheel analysis and protomer model of RII$\alpha$-(1–44).** *A*, the amino acid residues comprising helices I and II are mapped on $\alpha$-helical wheel projections. The residues are represented by *single-letter codes*. Hydrophobic residues are represented as *filled circles*. Residues 23 and 28, the last and first residues of helices I and II, are indicated. Observed NOE cross-peaks between Val$^{20}$ and Phe$^{31}$ are represented by a *dashed line*. The sequence Pro$^{25}$-Leu$^{28}$ comprises a turn. *B*, predicted protomer model of RII$\alpha$-(1–44). All residues located in the turn regions are indicated. Residues Ile$^{3}$ and Ile$^{5}$, both necessary for AKAP binding, are shown on the $\beta$-strand. Also shown are residues Val$^{20}$ and Phe$^{31}$ which make a proposed intrasubunit contact.

causing minor conformational changes. A structural model in which the helix turn helix motif of the monomer packs in an anti-parallel arrangement with its partner in the dimer to form a four-helix bundle explains both the mutagenesis and NOE data. The quaternary structure and orientation of the $\beta$-strand with respect to the helical core in RII$\alpha$ is currently under investigation and will delineate the true conformation of the domain.

*Acknowledgments*—We gratefully acknowledge Dr. Larry Gross for electrospray ionization-mass spectrometric analysis, Drs. David Eleizer, Mark Foster, Ishwar Radhakrishnan, Vince Coghlan, and Alan Deese for helpful discussions and Dr. Alexandra Newton for a critical reading of the manuscript. We thank Dr. Peter Wright for the use of his CD spectropolarimeter. We appreciate the guidance of Dr. Joseph P. Noel during the dynamic light scattering measurements.

REFERENCES

1. Taylor, S. S., Buechler, J. A., and Yonemoto, W. (1990) *Annu. Rev. Biochem.* **59,** 971–1005
2. Meinkoth, J. L., Alberts, A. S., Went, W., Fantozzi, D., Taylor, S. S., Hagiwara, M., Montminy, M., and Feramisco, J. R. (1993) *Mol. Cell. Biochem.* **127–128,** 179–186
3. Scott, J. D. (1991) *Pharmacol. Ther.* **50,** 123–145
4. Gill, G. N. (1995) *Structure* **3,** 1285–1289
5. Newton, A. C. (1995) *J. Biol. Chem.* **270,** 28495–28498
6. Pawson, T. (1995) *Nature* **373,** 573–580
7. Scott, J. D., and McCartney, S. (1994) *Mol. Endocrinol.* **8,** 5–11
8. Faux, M. C., and Scott, J. D. (1996) *Cell* **85,** 9–12
9. Rubin, C. S. (1994) *Biochim. Biophys. Acta* **1224,** 467–479
10. Dell'Acqua, M. L., and Scott, J. D. (1997) *J. Biol. Chem.* **272,** 12881–12884
11. Newton, A. C. (1996) *Curr. Biol.* **6,** 806–809
12. Faux, M. C., and Scott, J. D. (1996) *Trends Biochem. Sci.* **21,** 312–315
13. Levin, D. E., and Errede, B. (1995) *Curr. Opin. Cell Biol.* **7,** 197–202
14. Coghlan, V. M., Perrino, B. A., Howard, M., Langeberg, L. K., Hicks, J. B., Gallatin, W. M., and Scott, J. D. (1995) *Science* **267,** 108–111
15. Nauert, J. B., Klauck, T. M., Langeberg, L. K., and Scott, J. D. (1996) *Curr. Biol.* **7,** 52–62
16. Carr, D. W., Stofko-Hahn, R. E., Fraser, I. D. C., Bishop, S. M., Acott, T. S., Brennan, R. G., and Scott, J. D. (1991) *J. Biol. Chem.* **266,** 14188–14192
17. Carr, D. W., Hausken, Z. E., Fraser, I. D. C., Stofko-Hahn, R. E., and Scott, J. D. (1992) *J. Biol. Chem.* **267,** 13376–13382
18. Su, Y., Dostmann, R. G., Herberg, F. W., Durick, K., Xuong, N.-H., Ten Eyck, L., Taylor, S. S., and Varughese, K. I. (1995) *Science* **269,** 807–813
19. Hausken, Z. E., Coghlan, V. M., Hastings, C. A. S., Reimann, E. M., and Scott, J. D. (1994) *J. Biol. Chem.* **269,** 24245–24251
20. Luo, Z., Shafit-Zagardo, B., and Erlichman, J. (1990) *J. Biol. Chem.* **265,** 21804–21810
21. Aurell, L., Friberger, P., Karlsson, G., and Clauson, G. (1977) *Thromb. Res.* **11,** 595–609
22. Nagai, K., and Thøgersen, H. C. (1984) *Nature* **309,** 810–812
23. Gill, S. C., and von Hippel, P. H. (1989) *Anal. Biochem.* **182,** 319–326
24. Bax, A., and Davis, D. G. (1985) *J. Magn. Reson.* **65,** 355–360
25. Piotto, M., Saudek, V., and Sklenar, V. (1992) *J. Biomol. NMR* **2,** 661–665
26. Sklenar, V., Piotto, M., Leppik, R., and Saudek, V. (1993) *J. Magn. Reson.* **,** 241–245
27. Wishart, D. S., Bigam, C. G., Yao, J., Abildgaard, F., Dyson, H. J., Oldfield, E., Markley, J. L., and Sykes, B. D. (1995) *J. Biomol. NMR* **6,** 135–140
28. Marion, D., and Wüthrich, K. (1983) *Biochem. Biophys. Res. Commun.* **113,** 608–613
29. States, D. J., Haberkorn, R. A., J., and R. D. (1982) *J. Magn. Reson.* **48,** 286–292
30. Muhandiram, D. R., and Kay, L. E. (1994) *J. Magn. Reson.* **103,** 203–216
31. Kay, L. E., Keifer, P., and Saarinen, T. (1992) *J. Am. Chem. Soc.* **114,** 10663–10664
32. Schleucher, J., Sattler, M., and Griesinger, C. (1993) *Angew. Chem. Int. Ed. Engl.* **105,** 1518–1521
33. Jeener, T., Meier, B. H., Bachman, P., and Ernst, R. R. (1979) *J. Chem. Phys.* **71,** 4546–4553
34. Bodenhausen, G., and Ruben, D. J. (1980) *Chem. Phys. Lett.* **69,** 185–189
35. Mori, S., Abeygunawardana, C., Johnson, A. O., and van Zijl, P. C. M. (1995) *J. Magn. Reson.* **108,** 94–98
36. Marion, D., Driscoll, P. C., Kay, L. E., Wingfield, P. T., Bax, A., Gronenborn, A. M., and Clore, M. (1989) *Biochemistry* **28,** 6150–6156
37. Shaka, A. J., Keeler, L., Frenkiel, T., and Freeman, R. (1983) *J. Magn. Reson.* **52,** 335–338
38. Grzesiek, S., and Bax, A. (1992) *J. Am. Chem. Soc.* **114,** 6291–6293
39. Wittekind, M., and Mueller, L. (1993) *J. Magn. Reson.* **101,** 201–205
40. Ikura, M., Kay, L. E., and Bax, A. (1990) *Biochemistry* **29,** 4659–4667
41. Ikura, M., and Bax, A. (1991) *J. Biomol. NMR* **1,** 99–104
42. Bax, A., Clore, G. M., and Gronenborn, A. M. (1990) *J. Magn. Reson.* **88,** 425–431
43. Kay, L. E., Xu, G., Singer, A. U., Muhandiram, D. R., and Forman-Kay, J. D. (1993) *J. Magn. Reson.* **101,** 333–337
44. Patt, S. L. (1992) *J. Magn. Reson.* **96,** 94–102
45. McCoy, M. A., and Mueller, L. (1992) *J. Am. Chem. Soc.* **114,** 2108–2112
46. McCoy, M. A., and Mueller, L. (1992) *J. Magn. Reson.* **98,** 674–679
47. Johnson, W. C., Jr. (1985) *Methods Biochem. Anal.* **31,** 61–163
48. Johnson, W. C., Jr. (1990) *Proteins Struct. Funct. Genet.* **7,** 205–214
49. Venyaminov, S. Y., and Yang, J. T. (1996) in *Determination of Protein Secondary Structure. Circular Dichroism and the Conformational Analysis of Biomolecules* (Fasman, G. D., ed), Plenum Publishing Corp., New York
50. Carr, D. W., and Scott, J. D. (1992) *Trends Biochem. Sci.* **17,** 246–249
51. Scott, J. D., Stofko, R. E., McDonald, J. R., Comer, J. D., Vitalis, E. A., and Mangili, J. A. (1990) *J. Biol. Chem.* **265,** 21561–21566
52. Li, Y., and Rubin, C. S. (1995) *J. Biol. Chem.* **270,** 1935–1944
53. Spera, S., and Bax, A. (1991) *J. Am. Chem. Soc.* **113,** 5490–5492

54. Wishart, D. S., and Sykes, B. D. (1994) *J. Biomol. NMR* **4,** 171–180
55. Wishart, D. S., Sykes, B. D., and Richards, R. M. (1991) *J. Mol. Biol.* **222,** 311–333
56. Wishart, D. S., Sykes, B. D., and Richards, R. M. (1992) *Biochemistry* **31,** 1647–1651
57. Wüthrich, K. (1986) *NMR of Proteins and Nucleic Acids*, John Wiley & Sons, Inc., New York
58. Potts, B. C., Smith, J., Akke, M., Macke, T. J., Okazaki, K., Hidaka, H., Case, D. A., and Chazin, W. J. (1995) *Nat. Struct. Biol.* **2,** 790–796
59. Starich, M. R., Sandman, K., Reeve, J. N., and Summers, M. F. (1996) *J. Mol. Biol.* **33,** 15036–15045
60. Handel, T. M., and Domaille, P. J. (1996) *Biochemistry* **35,** 6569–6584
61. Burgering, M. J., Boelens, R., Gilbert, D. E., Breg, J. N., Knight, K. L., Sauer, R. T., and Kaptein, R. (1994) *Biochemistry* **33,** 15036–15045
62. Manning, M. C., and Woody, R. W. (1989) *Biochemistry* **28,** 8609–8613
63. Richardson, J. S., and Richardson, D. C. (1988) *Science* **240,** 1648–1652
64. Presta, L. G., and Rose, G. D. (1988) *Science* **240,** 1632–1641
65. Molday, R. S., Englander, S. W., and Kallen, R. G. (1972) *Biochemistry* **11,** 150–158
66. Bai, Y., Milne, J. S., Mayne, L., and Englander, S. W. (1993) *Proteins Struct. Funct. Genet.* **17,** 75–86
67. Connelly, G. P., Bai, Y., Jeng, M.-P., and Englander, S. W. (1993) *Proteins Struct. Funct. Genet.* **17,** 87–92
68. Brahmachari, S. K., Bhatnagar, R. S., and Ananthanarayanan, V. S. (1982) *Biopolymers* **21,** 1107–1125
69. Dyson, H. J., and Wright, P. E. (1991) *Annu. Rev. Biophys. Biophys. Chem.* **20,** 519–538
70. Shin, H.-C., Merutka, G., Waltho, J. P., Wright, P. E., and Dyson, H. J. (1993) *Biochemistry* **32,** 6348–6355
71. Shin, H.-C., Merutka, G., Waltho, J. P., Tennant, L. L., Dyson, H. J., and Wright, P. E. (1993) *Biochemistry* **32,** 6356–6364
72. Yao, J., Feher, V. A., Espejo, B. F., Reymond, M. T., Wright, P. E., and Dyson, H. J. (1994) *J. Mol. Biol.* **243,** 736–753
73. Hausken, Z. E., Dell'Acqua, M. L., Coghlan, V. M., and Scott, J. D. (1996) *J. Biol. Chem.* **271,** 29016–29022